Title

A mass-conservative predictor-corrector solution to the 1D Richards equation with adaptive time control

Authors

Li, Zhi
Özgen-Xian, Ilhan
Maina, Fadji Zaouna

Publication Date

2021

DOI

10.1016/j.jhydrol.2020.125809

A mass-conservative predictor-corrector solution to the 1D Richards equation with adaptive time control

Zhi Li[a,*], Ilhan Özgen-Xian[a], Fadji Zaouna Maina[a]

[a]*Energy Geosciences Division, Lawrence Berkeley National Laboratory, Berkeley, CA, USA*

Abstract

Predictor-corrector-type (P-C) numerical solution to the 1D Richards equation only requires one matrix inversion operation per time step, making it attractive in terms of computational cost. However, mass conservation could be violated at the saturated-unsaturated interface. A new post-allocation procedure is designed for the P-C method, which redistributes moisture after the corrector step to achieve strict mass balance. A novel adaptive time-stepping strategy is proposed to further improve model efficiency and robustness. It adjusts time step size based on both moisture difference and the Courant number. By testing against analytical solution, existing P-C solution and existing iterative solution, the new numerical solution shows good conservation property and efficiency. The new time-stepping strategy better balances computational cost and model accuracy because it takes the soil water retention relationship into consideration.

Keywords: Richards equation, mass conservation, predictor-corrector method, adaptive time control

1. Introduction

Richards equation (Richards, 1931) describes flow in unsaturated soils due to gravity and capillarity. Because it is widely used to model the variably saturated flow in physically-based hydrological models (Paniconi and Putti, 2015),

*Corresponding author
Email address: lizhi@lbl.gov (Zhi Li)

its numerical solution plays a key role in hydrology and environmental sciences. Unfortunately, the Richards equation is highly nonlinear, which makes its numerical solution computationally expensive, uncertain, and non-robust (Farthing and Ogden, 2017). This work presents an efficient numerical scheme for the one-dimensional Richards equation that reduces computational cost and enhances robustness.

Richards equation can be formulated in a head, water content, or mixed form—see Caviedes-Voullieme et al. (2013) for a detailed discussion of trade-offs. We will only discuss the mixed and the head forms in this manuscript, because the water content form is not relevant to our work. The one-dimensional mixed form of the Richards equation is given by:

$$\frac{S_s \theta}{\phi}\frac{\partial h}{\partial t} + \frac{\partial \theta}{\partial t} - \frac{\partial}{\partial z}\left[K(h)\left(\frac{\partial h}{\partial z} - 1\right)\right] - q_s = 0 \tag{1}$$

Here, S_s is specific storage, h is pressure head, θ is water content, ϕ is porosity, $K(h)$ is hydraulic conductivity and q_s represents source/sink terms. It is called the mixed form because both h and θ are considered primary variables. The head form can be derived from the mixed form by defining a specific capacity $C(h) = \partial\theta/\partial h$ and substituting $C(h)$ into Eq. (1), which yields:

$$\left(\frac{S_s \theta}{\phi} + C(h)\right)\frac{\partial h}{\partial t} - \frac{\partial}{\partial z}\left[K(h)\left(\frac{\partial h}{\partial z} - 1\right)\right] - q_s = 0 \tag{2}$$

The advantage of the head form is that it only involves h as the unknown, which is not bounded at saturation. However, the numerical solution of the head form does not conserve mass in the unsaturated zone (Lehmann and Ackerer, 1998; Caviedes-Voullieme et al., 2013), because the soil water retention relationship (i.e. the h-θ relationship) is highly nonlinear, which makes the time derivative $C(h)\partial h/\partial t$ to diverge from $\partial\theta/\partial t$ in its discrete form (Zha et al., 2017). An iterative numerical scheme by Celia et al. (1990) overcomes this issue. It uses a Taylor series expansion of water content to compensate for the mass loss and has become a widely used strategy to solve the head form of the Richards equation (Paniconi and Putti, 2015).

Kirkland et al. (1992) propose a non-iterative predictor-corrector-type (P-C) method to solve the Richards equation. A predictor step, which solves the head form, is followed by a corrector step, wherein the mixed form is solved to correct head values in the unsaturated zone. Lai and Ogden (2015) further improve this method using a post-allocation procedure to enforce mass conservation at the saturated-unsaturated interface, which redistributes the non-conserved fraction of moisture to nearby grid cells. In contrast to the iterative method by Celia et al. (1990), the P-C method only requires one matrix inversion per time step. This makes the P-C method competitive in terms of computational cost.

The aim of the present study is to further improve the P-C method by identifying its capabilities and limitations. We improve the P-C method proposed by Lai and Ogden (2015) to address the following issues: (i) the post-allocation procedure is conservative only when an unsaturated capacity exists; (ii) the computational cost of the P-C method has not yet been compared to iterative methods.

The first point concerning the post-allocation procedure acknowledges that moisture cannot be redistributed between fully saturated grid cells, because there is no space to accommodate excess water. This limitation is relevant for catchment-scale studies, which commonly use impermeable bottom boundaries (e.g. Camporese et al., 2015; Sun et al., 2016; Weill et al., 2013). In these studies, fully saturated regions exist near the impermeable bottom or below the water table. When excess moisture is sent to these regions from the upper unsaturated zone, it has to be abandoned to guarantee the saturated water content is not exceeded, thus resulting in an inaccurate mass balance.

The second point concerning the computational cost reflects on the fact that the iterative scheme becomes more efficient than the non-iterative P-C method if the time step size (Δt) of the P-C method is too restrictive. Numerical solutions of the Richards equation often adopt variable Δt (Zha et al., 2019). For iterative methods, Δt is usually constrained by monitoring the number of iterations it takes for the current step to converge (D'Haese et al., 2007; Maina and Ackerer, 2017). Here, if the number of iterations exceeds a certain threshold, Δt is reduced. For non-iterative methods, there is no single optimal strategy to constrain Δt. While Δt can be adjusted based on the maximum change of water content (Lai and Ogden, 2015) or the truncation error of the time derivative (Kavetski et al., 2002), a mixed use of multiple criteria is often required (D'Haese et al., 2007). Because the P-C method uses an explicit time integration for the corrector step, it might require an additional stability criterion that further limits the maximum time step size $\Delta t_{\max}$ (Lai and Ogden, 2015). Several approaches have been suggested to limit $\Delta t_{\max}$. For example, El-Kadi and Ling (1993) apply a Kirchhoff transformation to the Richards equation, obtaining a new form that is similar to an advection-diffusion equation. Stability criteria can then be established using the Courant (Co) and Peclet (Pe) numbers as commonly performed for degenerate hyperbolic-parabolic shallow flow equations in surface hydraulics (for example, Li and Hodges, 2019). Because the recommended Co and Pe values in El-Kadi and Ling (1993) are based on a literature review rather than a stability analysis of the Kirchhoff transform, whether these values are optimal remains unclear. Assuming linear behavior of soil parameters and a minimum bound for the length of the observable discrete wave, Caviedes-Voullieme et al. (2013) carry out a von Neumann stability analysis to constrain Δt. This results in a time step constrain of order $O(h^2)$, which is to be expected for diffusion-type equations (for example, Hirsch, 2007). Due to the strong assumptions taken to cope with nonlinearity, this stability criterion might be too restrictive in some cases—see Hunter et al. (2005) for similar arguments.

In this work, we (i) present modifications to the post-allocation procedure to conserve mass when moisture redistribution within fully saturated regions occur; and (ii) apply various time control strategies to the P-C method and derive a novel adaptation strategy for Δt, which combines the use of an empirical Courant number and the water content criterion from Lai and Ogden (2015). We compare our novel P-C method (named P-C-A for predictor-corrector-allocation) with the P-C method from Lai and Ogden (2015) and an iterative method to assess its robustness and computational efficiency.

The next sections are organized as follows: Section 2 introduces the P-C method (Lai and Ogden, 2015), the new post-allocation procedure and the new time control scheme. Section 3 describes the test problems and results. Section 4 discusses in detail the reasons behind the observed results as well as directions for future research. Section 5 concludes the findings.

2. Methods

2.1. The predictor-corrector method

We briefly sketch out the predictor-corrector (P-C) method—see Lai and Ogden (2015) for a more detailed description. In the predictor step, the head form of the Richards equation (Eq. 2) is discretized as (neglect source term):

$$\begin{aligned}&\left[C(h_i^n) + \frac{S_s\theta_i^n}{\phi}\right](h_i^* - h_i^n)\\&\quad - \frac{K(h_{i+\frac{1}{2}}^n)\Delta t}{\Delta z_i \Delta z_{i+\frac{1}{2}}}\left(h_{i+1}^* - h_i^*\right) + \frac{K(h_{i-\frac{1}{2}}^n)\Delta t}{\Delta z_i \Delta z_{i-\frac{1}{2}}}\left(h_i^* - h_{i-1}^*\right)\\&\quad + \frac{K(h_{i+\frac{1}{2}}^n)\Delta t}{\Delta z_i} - \frac{K(h_{i-\frac{1}{2}}^n)\Delta t}{\Delta z_i} = 0 \qquad (3)\end{aligned}$$

where the subscript i indicates spatial coordinates (cell-centered, increasing downward) and superscript n indicates time level. The variable h^* is an intermediate solution, which does not ensure mass conservation. The grid size Δz is indexed to allow potential use of variable spatial resolution, but fixed Δz is applied in the present study.

The Mualem–van Genuchten model (Mualem, 1976; van Genuchten, 1980) is used to link pressure head with water content and hydraulic conductivity:

$$S(h) = (1 + |\alpha h|^n)^{-m} \tag{4}$$

$$\theta(h) = \theta_r + (\theta_s - \theta_r) S(h) \tag{5}$$

$$K(h) = K_s S(h)^{\frac{1}{2}} \left[1 - \left(1 - S(h)^{\frac{1}{m}}\right)^m\right]^2 \tag{6}$$

where, S represents saturation, α and n are soil parameters, $m = 1 - 1/n$, θ_s and θ_r are saturated and residual water contents, K_s is the saturated hydraulic conductivity. The specific capacity can be derived as:

$$C(h) = \frac{\alpha n m (\theta_s - \theta_r) |\alpha h|^{n-1}}{(1 + |\alpha h|^n)^{m+1}} \tag{7}$$

For fully saturated soil, we have $S = 1$, $\theta = \theta_s$, $K = K_s$ and $C = 0$. The interface conductivity, for example, $K_{i+\frac{1}{2}}$ at the interface $i + \frac{1}{2}$, is calculated as the arithmetic mean of the two neighboring cell-centered values as suggested by Lai and Ogden (2015); van Dam and Feddes (2000).

Eqs. (3–7) can be combined to form a tri-diagonal linear system, which can be solved to obtain h^*. Then, a corrector step to enforce mass conservation is performed by solving the mixed form of the Richards equation (Eq. 1). The flux between two grid cells is estimated with Darcy's Law:

$$q^*_{i+\frac{1}{2}} = \frac{K(h^*_{i+\frac{1}{2}})}{\Delta z_{i+\frac{1}{2}}} \left(h^*_{i+1} - h^*_i\right) - K(h^*_{i+\frac{1}{2}}) \tag{8}$$

The water content is updated by substituting Eq. (8) into the mixed form equation (neglect source term):

$$\theta^*_i + \frac{S_s \theta^*_i}{\phi} (h^*_i - h^n_i) = \theta^n_i - \frac{\Delta t}{\Delta z_i} \left(q^*_{i-\frac{1}{2}} - q^*_{i+\frac{1}{2}}\right) \tag{9}$$

Since h^* has been solved via Eq. (3), the corrector step is fully explicit. The water content calculated from Eq. (9), θ^*, is not the final value. The modeler needs to decide whether the head form (Eq. 3) or the mixed form (Eq. 9) solution will be used; in other words, whether h^* or θ^* is the solution at the new time level. Lai and Ogden (2015) listed three cases based on the saturation status and position of a grid cell i:

1. If cell i is unsaturated and is not adjacent to a saturated cell, set $\theta_i^{**} = \theta_i^*$. The head $h_i^{n+1} = h(\theta_i^{**})$ is calculated by inverting Eq. (4) and (5).
2. If cell i is unsaturated and is adjacent to a saturated cell, set $h_i^{n+1} = h_i^*$. If Eq. (4) and (5) give a water content $\theta(h_i^{n+1}) > \theta_i^*$, then set $\theta_i^{**} = \theta(h_i^{n+1})$ and fill the gap by extracting water from its upwind cell.
3. If cell i is over-saturated, set $h_i^{n+1} = h_i^*$, $\theta_i^{**} = \theta_s$ and send excess water to its downwind cell.

The entire solution procedure can be summarized as *predict* (get h^*) – *correct* (get θ^*) – *select* (get h^{n+1} and θ^{**}) – *allocate* (get θ^{n+1}). Here, the last two steps can be grouped together as the *post-allocation step*.

2.2. Improved moisture allocation procedure

In the absence of unsaturated adjacent cells, the P-C method may still violate mass conservation when a grid cell switches its saturation status. In this section, we present an improved allocation procedure that satisfies mass conservation under all circumstances.

The novel post-allocation procedure is illustrated in the flowchart in Fig. 1. We summarize:

1. If cell i is unsaturated and is not adjacent to a saturated cell, set $\theta_i^{**} = \theta_i^*$. The head $h_i^{n+1} = h(\theta_i^{**})$ is calculated by inverting Eq. (4) and (5).
2. If cell i is unsaturated and is adjacent to a saturated cell, set $h_i^{n+1} = h_i^*$. The corresponding water content is computed from the water retention relation, i.e. $\theta^{**} = min\left[\theta_s, \theta(h^{n+1})\right]$.
3. If cell i is over-saturated, set $h_i^{n+1} = h_i^*$, $\theta_i^{**} = \theta_s$.
4. Whenever the head form is accepted ($h_i^{n+1} = h_i^*$), the difference between θ^* and θ^{**} needs to be sent to or extracted from (depending on its sign) nearby cells to satisfy conservation.

An example algorithm that sends an excess amount of moisture ($\Delta\theta_i = \theta_i^* - \theta_i^{**}$) to the downward cells is provided as function *send_down* in Algorithm 1. Similar algorithms can be used for *send_up*, *extract_down* and *extract_up*.

Algorithm 1: Function - *send_down*(θ^{**}, $\Delta\theta_i$, i)

input : Water content θ^{**}, Cell index i, Moisture deficit $\Delta\theta_i$

output: Water content θ^{***}, Remaining moisture $\delta\theta_i$

$j = i + 1;$

while $\Delta\theta_i > 0$ *and* $j \leq N$ **do**

  $\omega = min(\Delta\theta_i, \theta_s - \theta_j^{**});$

  $\theta_j^{***} = \theta_j^{**} + \omega;$

  $\Delta\theta_i = \Delta\theta_i - \omega;$

  $j = j + 1;$

end

$\delta\theta_i = \Delta\theta_i$

In Algorithm 1, the moisture deficit $\Delta\theta_i$ is sent successively to all downwind cells until the remaining deficit is zero or the bottom of the domain is reached. Here, θ_i^{***} represents an intermediate water content for cell i after it sent or received moisture. θ_i^{***} is not the final water content, because cell i might continue to send or receive moisture from other cells. After all post-allocation steps are completed for all grid cells, the water contents are updated to θ^{n+1}.

The main differences between our improved post-allocation procedure and the original one (Lai and Ogden, 2015) are summarized in Table 1. Our procedure checks for unsaturated capacity before allocating excess moisture, $\Delta\theta$, and does not limit the redistribution to the adjacent cell only. If the adjacent cell does not have enough space, after filling the adjacent cell, the remaining excess moisture is sent further downwind. If excess moisture still exists after reaching the downwind boundary (that is, $\delta\theta > 0$), the remaining moisture is sent back to the upwind cells. Extracting moisture follows a similar pattern to sending moisture. Unlike in Lai's original method, where allocation is performed once for each grid cell, the new procedure may allocate moisture multiple times for one grid cell until $\delta\theta$ is zero.

Furthermore, Lai's original procedure only sends moisture from over-saturated grid cells. Our procedure sends moisture whenever a positive moisture deficit $\Delta\theta_i$ is detected. It will be shown in Sec. 4 that sending $\Delta\theta$ from unsaturated cells should not be neglected.

Table 1: Differences between the post-allocation procedure by Lai (P-C) and the new allocation strategy (P-C-A)

Mechanism	P-C	P-C-A
Check for unsaturated capacity	No	Yes
Redistribute within adjacent cells only	Yes	No
Send $\Delta\theta_i$ when $\theta_i^* \geq \theta_s$, $\Delta\theta_i > 0$	Yes	Yes
Send $\Delta\theta_i$ when $\theta_i^* < \theta_s$, $\Delta\theta_i > 0$	No	Yes
Extract $\Delta\theta_i$ when $\Delta\theta_i < 0$	Yes	Yes

The upwind/downwind direction is determined by the gradient of the total head, dH/dz (total head H is distinguished from pressure head h). For example, if $(dH/dz)_{i+\frac{1}{2}} < 0$ and $(dH/dz)_{i-\frac{1}{2}} < 0$, meaning that flow is downward at cell i, moisture is sent down or extracted from up. A special case exists where the total head gradients at the cell faces are of opposite signs, i.e. $(dH/dz)_{i+\frac{1}{2}}(dH/dz)_{i-\frac{1}{2}} < 0$. In this case, $\Delta\theta_i$ is split in both directions and the fraction of $\Delta\theta_i$ in each direction is determined by the relative magnitudes of each head gradient.

Hereinafter, Lai's original method (Sec. 2.1) is referred to as the P-C method. The P-C method with our novel post-allocation scheme (Sec. 2.2) is referred to as the P-C-A method.

2.3. Adaptive time stepping

A variable time step (Δt) is often used to solve the Richards equation in order to improve the computational efficiency. For example, Lai and Ogden

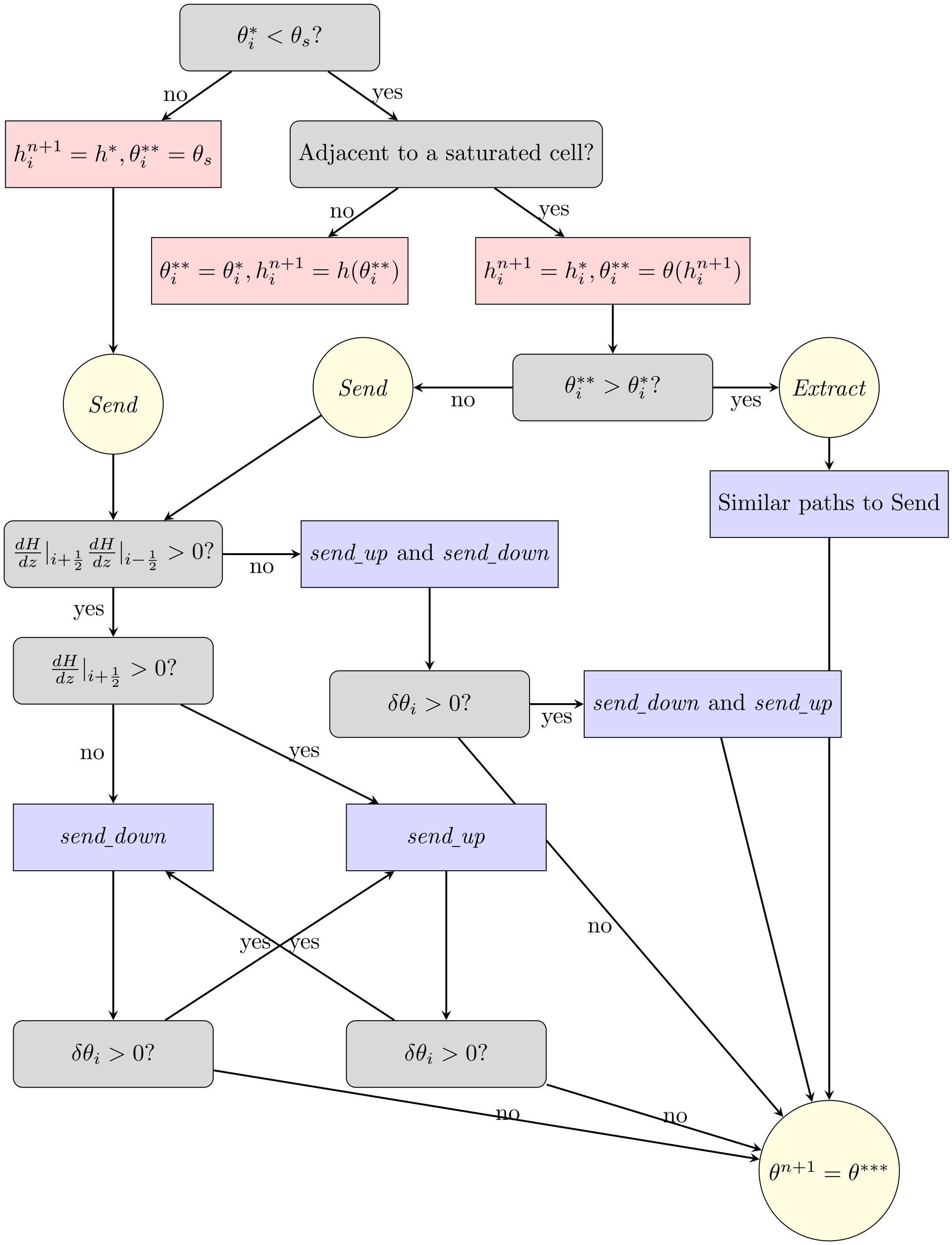

Figure 1: New post-allocation flowchart. *send_down* and *send_up* are functions that send excess moisture to nearby cells (see Algorithm 1). The *Extract* operations are similar to *Send*, so they are not expanded in detail.

(2015) adjust Δt based on the change in moisture content during the corrector step, namely:

$$\Delta\theta^*_{\max} = max_i(\theta^*_i - \theta^n_i) \tag{10}$$

$$\Delta t^{n+1} = \begin{cases} max(\Delta t^n r_{\text{red}}, \Delta t_{\min}), & \text{if } \Delta\theta^*_{\max} > \Theta_{\max} \\ min(\Delta t^n r_{\text{inc}}, \Delta t_{\max}), & \text{if } \Delta\theta^*_{\max} < \Theta_{\min} \\ \Delta t^n, & \text{otherwise} \end{cases} \tag{11}$$

where, $\Theta_{\max} = 0.02$ and $\Theta_{\min} = 0.01$ are threshold values determining when time step needs to be changed and $r_{\text{red}} = 0.9$, $r_{\text{inc}} = 1.1$ are coefficients determining how much the time step is to be changed. To avoid instability or impractical computational cost, the new time step Δt^{n+1} is limited within the user-defined range $[\Delta t_{\min}, \Delta t_{\max}]$.

One issue of using Eq. (11) is that the selections of $\Theta_{\max}$, $\Theta_{\min}$, r_{red}, r_{inc}, $\Delta t_{\min}$ and $\Delta t_{\max}$ are somewhat arbitrary. For model domains with different soil characteristics and boundary conditions, it is difficult to determine optimal values for these parameters without extensive trial and error. Another popular strategy to adjust Δt is to use the truncation error of the unsteady term (Kavetski et al., 2002; Maina and Ackerer, 2017). The truncation error is defined as:

$$\epsilon_t^{n+1} = \frac{1}{2}\Delta t^{n+1} max_i \left| \frac{h_i^{n+1} - h_i^n}{\Delta t^{n+1}} - \frac{h_i^n - h_i^{n-1}}{\Delta t^n} \right| \tag{12}$$

The time step is adjusted according to the following criteria:

$$\Delta t^{n+1} = \begin{cases} \Delta t^n min\left(s\sqrt{\frac{\epsilon_0}{max(\epsilon_t^{n+1}, \epsilon_{mech})}}, (r_t)_{\max}\right), & \text{if } \epsilon_t^{n+1} < \epsilon_0 \\ \Delta t^n max\left(s\sqrt{\frac{\epsilon_0}{max(\epsilon_t^{n+1}, \epsilon_{mech})}}, (r_t)_{\min}\right), & \text{otherwise} \end{cases} \tag{13}$$

where, s, ϵ_0,ϵ_{mech}, $(r_t)_{\min}$ and $(r_t)_{\max}$ are all user-defined parameters. A guidance on determining the values for these parameters is provided by Kavetski et al. (2002). The present study uses $s = 0.9$, $\epsilon_0 = 1 \times 10^{-3}$,$\epsilon_{mech} = 1 \times 10^{-9}$, $(r_t)_{\min} = 0.1$ and $(r_t)_{\max} = 4$.

The P-C and P-C-A methods differ from other prevailing numerical schemes in that the corrector step is fully explicit, which might impose additional limits on Δt for stability reasons. By using the Kirchhoff transformation, El-Kadi and Ling (1993) showed that the transformed Richards equation shares a similar form with the advection-diffusion equation, whose stability is reflected from the Peclet number (Pe) and the Courant number (Co). These two dimensionless numbers are defined as:

$$Pe = \frac{\Delta z}{K}\frac{dK}{dh}, \quad Co = \frac{\Delta t}{\Delta z}\frac{dK}{d\theta} \tag{14}$$

El-Kadi and Ling (1993) suggested to use Pe$<$ 0.5 and Co$<$ 2 as the stability criteria for the Richards equation. Note that only Co is a function of Δt. In the present study where sensitivity to the grid spacing (Δz) is not extensively investigated (we use fixed Δz), Pe is not used.

With the Courant number, the maximum allowable time step can be derived as:

$$\Delta t_{\mathrm{maxCo}} = Co_{\max} \Delta z \left(\frac{dK}{d\theta}\right)^{-1} \tag{15}$$

where, $dK/d\theta$ is derived analytically from Eq. (4) to (6):

$$\begin{aligned}\frac{dK}{dS} =& \frac{1}{2} K_z S^{-\frac{1}{2}} \left(1 - \left(1 - S^{\frac{1}{m}}\right)^m\right)^2 \\ &+ 2K_z S^{\frac{2-m}{2m}} \left(1 - \left(1 - S^{\frac{1}{m}}\right)^m\right) \left(1 - S^{\frac{1}{m}}\right)^{m-1} \qquad (16)\\ \frac{dK}{d\theta} =& \frac{dK}{dS}\frac{dS}{d\theta} = \frac{dK}{dS}\frac{1}{\theta_s - \theta_r} \qquad (17)\end{aligned}$$

In the present study, Eq. (15) is used together with Eq. (11) in a way where the minimum between $\Delta t_{\mathrm{maxCo}}$ and $\Delta t_{\max}$ in Eq. (11) is used as the maximum allowable Δt, that is:

$$\Delta t^{n+1} = \begin{cases} max(\Delta t^n r_{\text{red}}, \Delta t_{\text{min}}), & \text{if } \Delta\theta^*_{\text{max}} > \Theta_{\text{max}} \\ min(\Delta t^n r_{\text{inc}}, \Delta t_{\text{max}}, \Delta t_{\text{maxCo}}), & \text{if } \Delta\theta^*_{\text{max}} < \Theta_{\text{min}} \text{ and } \theta^*_{\text{imax}} < \lambda\theta_s \\ min(\Delta t^n r_{\text{inc}}, \Delta t_{\text{max}}), & \text{if } \Delta\theta^*_{\text{max}} < \Theta_{\text{min}} \text{ and } \theta^*_{\text{imax}} \geq \lambda\theta_s \\ \Delta t^n, & \text{otherwise} \end{cases} \tag{18}$$

where, θ^*_{imax} is the water content θ^* for the cell where $\Delta\theta^*_{\text{max}}$ is obtained. Note that the use of Δt_{maxCo} is disabled when $\theta^*_{\text{imax}} \geq \lambda\theta_s$ because:

1. In saturated regions ($\theta^*_{\text{imax}} = \theta_s$), solution of the explicit corrector step is rejected (Fig. 1) and stability is no longer a concern.
2. In nearly saturated regions ($\theta_s > \theta^*_{\text{imax}} \geq \lambda\theta_s$), the Courant number increases abruptly (Fig. 2), which puts a stringent limit on Δt_{maxCo}.

Therefore, $\lambda \leq 1$ acts as a safety factor that avoids Δt_{maxCo} becoming too small. The present study uses $\lambda = 0.9999$. It should be noted that although El-Kadi and Ling (1993) recommend $Co_{\text{max}} = 2$, this value is not analytically derived and it only acts as a guideline. Nevertheless, it still narrows down the scope of selection by orders of magnitudes (selecting Δt_{max} in Eq. 11 could be purely random).

3. Numerical test cases

The proposed P-C-A method is first validated against the Warrick's analytical solution (Warrick et al., 1985). Then it is tested on a synthetic soil column with 6 different initial and boundary conditions to fully understand its behavior and assess its efficiency. Sensitivities to various adaptive time control strategies are also investigated. The results are also compared with that simulated by Hydrus-1D (Simunek et al., 2009), which is a finite element solver based on lumped Picard iterative method (Celia et al., 1990).

Table 2 lists parameters used for the Warrick and Synthetic test problems. 250 The present study does not investigate model sensitivity to different soil characteristics. The soil parameters are chosen based on the drainage test in Lai and Ogden (2015). The $Co - \theta$ relations can be visualized in Fig. 2. Note that this curve increases rapidly near saturation, which supports the use of the safety factor (λ) in Eq. (18).

Table 2: List of parameters

Symbol	Description	Value
$\Delta t^0[s]$	Initial time step	1×10^{-5}
θ_r	Residual water content	0
θ_s	Saturated water content	0.33
$K_s[m/s]$	Saturated conductivity	2.89×10^{-6}
$\alpha[1/m]$	Soil parameter	1.43
n	Soil parameter	1.56
$S_s[1/m]$	Specific storage	1×10^{-5}

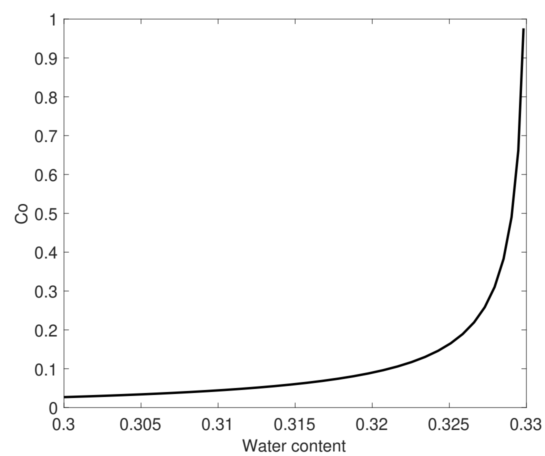

Figure 2: Courant number as a function of water content for the soil given in Table 2. The Courant number is estimated at $\Delta t = 100$ s.

3.1. Warrick's analytical solution

Warrick et al. (1985) proposed a generalized solution to the 1D infiltration problem, which has been widely used to validate Richards solvers (Caviedes-Voullieme et al., 2013; Phoon et al., 2007). The problem configuration consists of a soil column (1 meter deep) infiltrated with a constant head $h_{\text{top}} = 0$ m on top. A Neumann boundary condition (no flow) is imposed at the bottom of the domain. The initial water content is uniform in the domain and is $\theta^0 = 0.033$. With soil parameters listed in Table 2, this initial water content corresponds to a pressure head of -42.65 m. Detailed derivation of the Warrick's solution can be found in Phoon et al. (2007); Warrick et al. (1985) and is skipped here. In the present study, we first select proper values for Δt and Δz through grid and time step refinement tests. Then a comparison between the P-C and P-C-A results is performed to understand the effects of the proposed allocation scheme.

3.1.1. Sensitivity to Δt and Δx

Figure 3 shows simulation results for different values of $\Delta t_{\max}$ (Eq. 11 is used for adaptive time control). All the water content profiles in Fig. 3(a) are very similar and they all have good agreements with the analytical solution. But detailed examination near the saturated-unsaturated interface (Fig. 3b) reveals oscillatory behaviors. The oscillations can be reduced by using smaller $\Delta t_{\max}$, but they are never completely suppressed even with $\Delta t_{\max} = 0.05$ s (not obvious on the figure). Figure 3(c) shows the relative errors (ϵ_z) as functions of $\Delta t_{\max}$. The relative error for variable γ is estimated similar to the L_2-norm in Maina and Ackerer (2017):

$$\epsilon_\gamma = \left(\frac{1}{M} \sum_m \left| \frac{\gamma_m - \gamma_{\text{ref}}}{\gamma_{\text{ref}}} \right|^2 \right)^{\frac{1}{2}} \tag{19}$$

where, M is the total number of samples ($M = 9$ for the Warrick's problem in the present study), γ_{ref} is the reference value for this variable. Since the analytical solution in Fig. 3(a) is derived along the wetting front with large moisture gradient, we use $\gamma = z$ (rather than $\gamma = \theta$) for evaluating errors to minimize interference from interpolation. It can be seen from Fig. 3(c) that ϵ_z with respect to the analytical solution becomes stable when $\Delta t_{\max} \leq 0.2$ s. At this time step, the Hydrus-1D produces similar error with the P-C-A method.

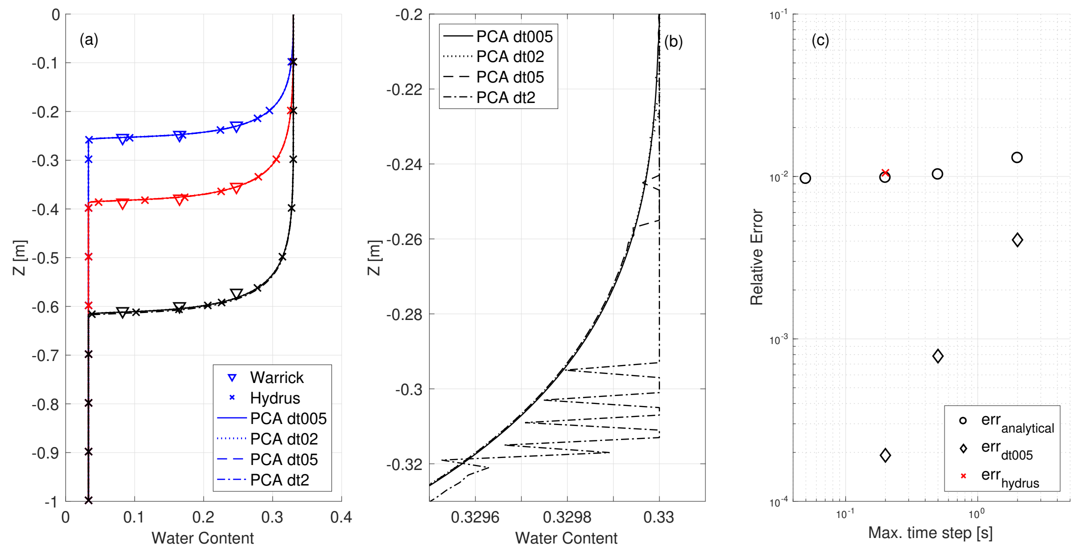

Figure 3: (a): Water content profiles for the Warrick problem with $\Delta t_{\max} = 0.05, 0.2, 0.5, 2$ s. The Hydrus results are plotted at a coarser spatial resolution for readability. Blue: 11700 s, Red: 23400 s, Black: 46800 s. (b): Same profiles but zoomed to the saturated-unsaturated interface. (c): Model errors (ϵ_z) estimated as the L_2-norm (Maina and Ackerer, 2017). Circle represents P-C-A error with respect to the analytical solution (γ_{ref} in Eq. 19 equals z from the analytical solution). Diamond represents P-C-A error with respect to $\Delta t_{\max} = 0.05$ s (γ_{ref} equals z from PCA dt005 simulation). Cross is the Hydrus error with respect to the analytical solution. These simulations are executed with $\Delta z = 0.2$ cm.

Figure 4 shows the results for different grid resolutions. Unlike Fig. 3(a) where all water content profiles overlap with each other, the profiles in Fig. 4(a) are affected by Δz. This phenomenon supports the viewpoint of Caviedes-Voullieme et al. (2013) who state that using small Δz should have higher priority than using small Δt. The zoomed profiles (Fig. 4b) show stronger oscillations for smaller Δz, indicating a reduction in Δt is required when grid resolution is refined. For the error plot in Fig. 4(c), minimal error is achieved at $\Delta z = 0.2$ cm. Further reducing the grid resolution slightly increases the model error.

Combining Fig. 3 and 4 together, we use $\Delta t_{\max} = 0.2$ s, $\Delta z = 0.2$ cm as the reference P-C-A configuration in the following sections.

Note that solution of this reference simulation is not completely oscillation-free, but the oscillations are too weak to be noticed even in the zoomed profile (Fig. 3b). In fact, all the oscillations are generally negligible if we look at the full water content profiles in Fig. 3(a) and 4(a). Caviedes-Voullieme et al. (2013) tried to reproduce the Warrick's solution with an explicit scheme, but reported instability at 46800 s. The P-C-A method, however, remains stable under minor oscillations. Thus we believe the P-C-A simulation with $\Delta t_{\max} = 0.2$ s, $\Delta z = 0.2$ cm can be used as reference.

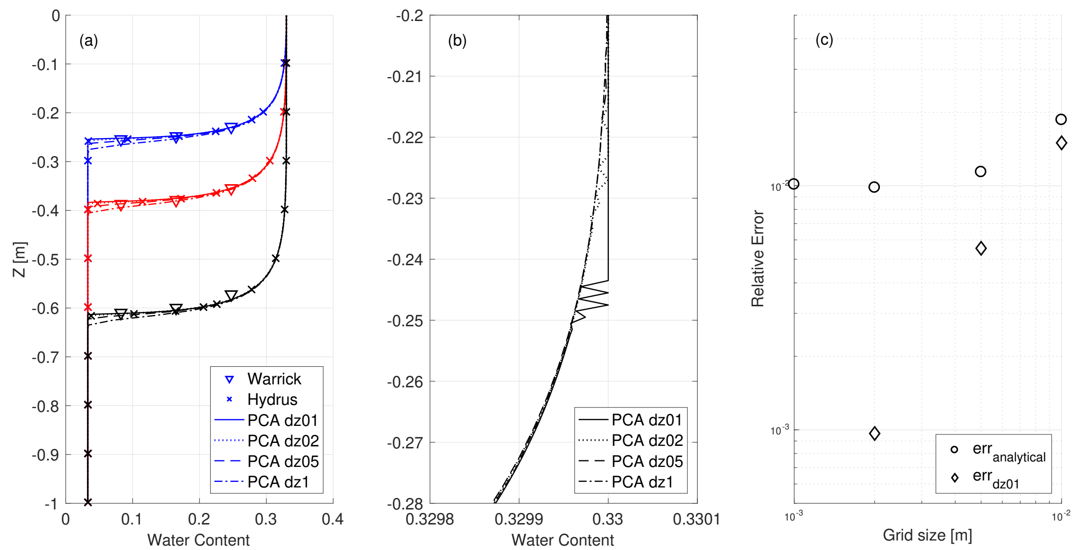

Figure 4: (a): Water content profiles for the Warrick problem with $\Delta z = 0.1, 0.2, 0.5, 1$ cm. The Hydrus results are plotted at a coarser spatial resolution for readability. Blue: 11700 s, Red: 23400 s, Black: 46800 s. (b): Same profiles but zoomed to the saturated-unsaturated interface. (c): Model errors (ϵ_z) estimated as the L_2-norm (Maina and Ackerer, 2017). Circle represents P-C-A error with respect to the analytical solution (γ_{ref} equals z from the analytical solution). Diamond represents P-C-A error with respect to $\Delta z = 0.1$ cm (γ_{ref} equals z from PCA dz01 simulation). These simulations are executed with $\Delta t_{\max} = 0.2$ s.

3.1.2. Comparison between P-C and P-C-A

With $\Delta z = 0.2$ cm, $\Delta t_{\max} = 0.2$ s from Sec. 3.1.1, the performance of P-C and P-C-A methods are compared in Fig. 5. No visible difference is observed between the two scenarios from the water content profiles in Fig. 5(a). A zoomed examination in Fig. 5(b) suggests slightly faster propagation of the infiltration front for the P-C-A method. The reason for this difference in infiltration speed can be found in Fig. 5(c), where the P-C method shows non-zero volume loss and positive relative mass error (RME) over time. The volume loss is estimated as the total amount of moisture truncated when enforcing over-saturated grid cells to exact saturation. The RME is defined as:

$$RME^{n+1} = 1 - \frac{\Delta z \sum_i \theta_i^{n+1}}{N \Delta z \theta^0 + \sum_{\tau=0}^{n+1} q_{in}^{\tau} - \sum_{\tau=0}^{n+1} q_{out}^{\tau}} \tag{20}$$

where, N is the number of grid cells, q_{in} and q_{out} are the flux in and out of the computational domain. The positive RME curve verifies the P-C method being non-conservative. The increasing volume loss indicates that the non-conservation can be contributed to truncating excess moisture for over-saturated cells. Recall that the post-allocation scheme of Lai and Ogden (2015) sends excess moisture from the over-saturated cells to their downwind cells, meaning that the excess moisture in over-saturated cells is not completely ignored, but they did not consider the situation where the downwind cell is also saturated. This negligence invalidates their post-allocation procedure when an unsaturated downwind cell does not exist. Figure 5(c) also shows the total volume redistributed during the post-allocation steps, which is estimated as $\sum_i (\theta_i^{n+1} - \theta_i^*) \Delta z$. The P-C-A simulation shows continuous moisture allocation during the entire infiltration process. The P-C simulation stops allocating moisture at about 2.7×10^4 s. The decrease and vanish of allocated volume corresponds to an increase of volume loss and RME. It further verifies that the conservation issue of the P-C method is related to its post-allocation scheme. On the contrary, the P-C-A simulation with the new allocation scheme (Fig. 1) is strictly conservative with zero RME.

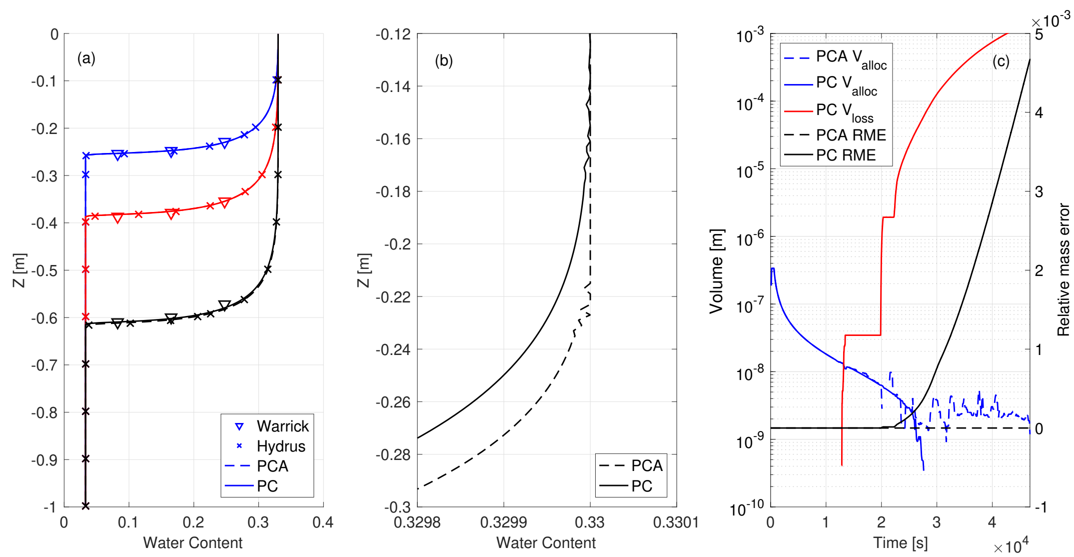

Figure 5: (a): Water content profiles for the Warrick problem with $\Delta z = 0.2$ cm, $\Delta t_{\max} = 0.2$ s. The Hydrus results are plotted at a coarser spatial resolution for readability. Blue: 11700 s, Red: 23400 s, Black: 46800 s. (b): Same profiles but zoomed to the saturated-unsaturated interface. (c): Blue: Volume changes during post-allocation, Red: Volume loss for P-C method. Black: Relative mass error (Eq. 20).

The relative errors for P-C and P-C-A simulations with respect to the analytical solution are 6.9×10^{-3} and 9.8×10^{-3}. Although the P-C method seems to produce lower error, detailed examination (not shown) reveals that the P-C error is partially neutralized by the volume loss. This serendipitous neutralization does not weaken the superiority of the P-C-A method over the P-C method.

3.2. Synthetic soil column

The P-C-A method is further tested using a 0.4-m synthetic 1D soil column with $\Delta z = 0.2$ cm. Six test scenarios are simulated to understand model behavior under various field conditions (Table 3). These scenarios are named using its top and bottom boundary conditions, which could be no flow (N), constant evaporation flux (E), constant infiltration flux (I) and constant head (H). In the first scenario (NN), the column is initially unsaturated and is sealed on both ends. After some time, the column reaches steady state under gravity and the bottom region becomes fully saturated. The second scenario (EN) adds complexity by enforcing an evaporation flux on top, which is often required in hydrological applications (e.g. Maquin et al., 2017; Or et al., 2013). The third and fourth scenarios (IN and HN) simulate infiltration into relatively dry soil with constant flux and constant head respectively. The fifth scenario (NH) is similar to the free drainage test performed in Forsyth et al. (1995); Lai and Ogden (2015), where a constant head condition is used on the bottom. The last scenario (EH) is similar to NH, but with evaporation on top.

For each of the synthetic scenarios, six simulations are performed with different solution algorithms and time control strategies. They are summarized in Table 4. For Hydrus-1D with heuristic time control strategy, Δt is increased by r_{inc} if a time step takes less than 3 iterations to converge. If it takes more than 7 iterations, Δt is reduced by a factor of r_{red}. All simulations in Table 4 use a minimum time step of 1×10^{-5} s.

Table 3: List of synthetic test scenarios

Name	Initial θ	Top BC	Bottom BC
NN	0.315	$q_{\text{top}} = 0$	$q_{\text{bot}} = 0$
EN	0.315	$q_{\text{top}} = -2 \times 10^{-7}$ m/s	$q_{\text{bot}} = 0$
IN	0.03	$q_{\text{top}} = 2 \times 10^{-6}$ m/s	$q_{\text{bot}} = 0$
HN	0.03	$h_{\text{top}} = 0$ m	$q_{\text{bot}} = 0$
NH	0.33	$q_{\text{top}} = 0$	$h_{\text{bot}} = 0$
EH	0.33	$q_{\text{top}} = -2 \times 10^{-7}$ m/s	$h_{\text{bot}} = 0$

Table 4: Summary of 6 simulations performed for each test scenario. The PCA02 is used as reference for estimating errors of other simulations.

Label	Solver	Δt control	$\Delta t_{\max}[s]$	$Co_{\max}$
Hydrus	Picard iteration	Heuristic	20	N.A.
PCA02	P-C-A	Eq. (11)	0.2	N.A.
PC02	P-C	Eq. (11)	0.2	N.A.
PCA20	P-C-A	Eq. (11)	20	N.A.
PCAC2	P-C-A	Eq. (18)	20	2
PCAT	P-C-A	Eq. (13)	N.A.	N.A.

3.2.1. NN and EN scenarios

Figure 6 shows the head and water content profiles for the NN and EN scenarios at 28, 144 and 648 minutes. The left two columns are the entire profiles. Column (c) is the water content profiles zoomed in to the saturated-unsaturated interface. Column (d) is the relative difference in water content estimated using Eq. (19) with respect to PCA02. Here we do not use the term "error" because the reference solution (PCA02) is not strictly considered the "true solution" (although Sec. 3.1 has shown it produces small error). For the NN scenario, gravity drives the initially-constant head and moisture towards hydrostatic distributions. The initial water content ($\theta^0 = 0.315$) is close to saturation, so steady state is reached in a short time (around 144 min). The EN scenario shows similar trend at early stages, but under continuous evaporation, the moisture profile finally moves away from saturation.

For both NN and EN profiles, different time control strategies make indistinguishable discrepancies (including PC02, which is not shown) and they are all very similar to the Hydrus results. The only visible discrepancy comes from PCAT after zooming in, where it slightly underestimates water content evolution. This is likely due to a very large Δt, which will be discussed in detail in Sec. 3.2.4.

The NN scenario has zero flux on both ends, so its mass should remain constant during simulation. It turns out that this is the case for all the P-C-A simulations, but PC02 generates a relative mass error of 0.000001% at 648 minutes. If the P-C model is executed with $\Delta t_{\max} = 20$ s (not listed in Table 4), RME is increased to 0.000007%. Since the head and water content evolutions are relatively mild for NN scenario, the mass error is negligible and invisible from the water content profiles, but it still indicates the existence of non-conservation for P-C method when simulating flow towards fully saturated region near an impermeable bottom boundary.

Figure 6(d) shows that PC02 produces the lowest relative difference with respect to PCA02 – less than 10^{-10} for EN. Since PC02 and PCA02 use same time control strategy and $\Delta t_{\max}$, the relative difference of PC02 is purely due to non-conservation, which is negligible. The relative difference of PCA20 is slightly higher than PCAC2 at 144 min. PCAT produces the highest deviation from PCA02 in both scenarios. The different behaviors among these 3 simulations are due to different time control strategies used. This result indicates that Δt has more important influence on model performance than mass conservation for the NN and EN scenarios.

In both scenarios, the relative differences generally decrease with time. For PCAT, this is because an increasing head gradient at late times leads to higher truncation error (Eq. 12), which enforces small Δt. For PCA20 and PCAC2, the reason is that water content evolves towards stabilized (NN) or highly unsaturated (EN) patterns at late times. Both of them minimize saturated-unsaturated exchange. It will be shown in the following sections that such exchange has to be resolved with small Δt, so as the saturated-unsaturated exchange diminishes, large Δt is allowed. But PCA20 and PCAC2 limit the maximum Δt, meaning that the actual $\Delta t = \Delta t_{\max}$ is much less than the maximum allowable Δt in theory, so a declining model deviation is observed.

Unfortunately, an error analysis of Hydrus is not performed because (i) Hydrus-1D output only retains 4 digits for water content, which is too coarse to be compared with the P-C-A results, and (ii) under the absence of an analytical solution, it is difficult to assess which method (between P-C-A and Hydrus) is more accurate. The error analysis loses its significance.

3.2.2. IN and HN scenarios

The head and moisture profiles for the infiltration scenarios (IN and HN) are shown in Fig. 7(a) and (b). In both scenarios, evolution of the wetting front is generally captured and good agreements with the results obtained with Hydrus-1D are observed. Detailed examination near the top boundary shows oscillatory behavior for PCA20 and PCAC2 in both scenarios. However, the oscillations are triggered by different mechanisms. For the IN scenario where a constant flux (smaller that the saturated hydraulic conductivity) is applied on top, the

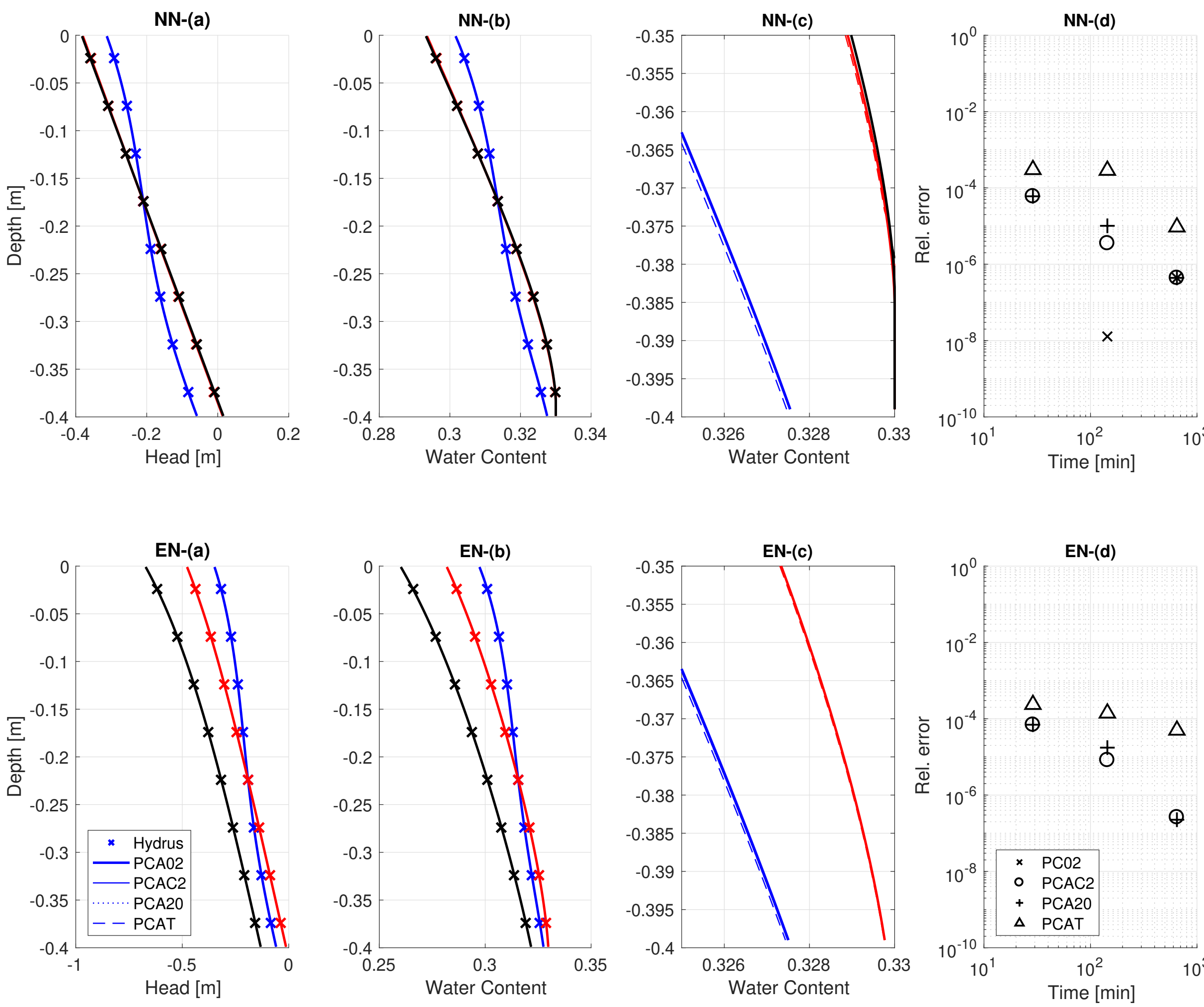

Figure 6: (a): Head and (b): water content profiles for NN and EN scenarios. Blue: $t = 28$ min, Red: $t = 144$ min, Black: $t = 648$ min. The Hydrus results are plotted at coarser resolution for readability. (c): Zoomed water content profiles to show details near the saturated-unsaturated interface. (d): Relative difference of water content (ϵ_θ) for the tested scenarios (taking PCA02 as the reference solution).

soil column remains unsaturated during infiltration. According to Fig. 1, no post-allocation process occurs and the oscillation is likely due to the use of large Δt when solving the mixed form equation explicitly. The fact that PCA20 and PCAC2 have identical oscillation patterns indicates the Courant number criteria is not invoked. For the HN scenario that is similar to the Warrick's problem, the oscillation occurs during saturated-unsaturated transitions. Owing to the Courant number, in HN the PCAC2 has much weaker oscillation than PCA20. The different oscillation patterns between IN and HN can be explained by the shape of the $Co-\theta$ curve (Fig. 2), where the Courant number increases rapidly when approaching saturation. For the IN scenario where the computational domain is fully unsaturated, the Courant number criteria becomes too loose (i.e. $\Delta t_{\mathrm{maxCo}} > \Delta t_{\mathrm{max}}$). Given that both IN and HN are not oscillation-free, $Co_{\mathrm{max}} = 2$ as recommended by El-Kadi and Ling (1993) is clearly not small enough for these 2 scenarios.

The relative differences shown in column (d) match the observations from the profiles. PCA20 has high deviations in both scenarios. PCAC2 is identical to PCA20 for IN, but less deviated for HN. PCAT has relatively low relative differences in both scenarios because large head gradient at the wetting front leads to large truncation error and very small Δt. PC02 produces the lowest relative differences that are less than 10^{-10}. In fact, the relative difference of PC02 is zero for IN scenario because when post-allocation is not invoked, PC02 is identical to PCA02. No estimation is made for HN at 648 min because the computational domain becomes fully saturated.

3.2.3. NH and EH scenarios

Figure 8 shows the head and moisture profiles for NH and EH scenarios that simulate drainage at the bottom. In both scenarios, good agreements for all test simulations are achieved in the upper part of the computational domain. Oscillations are observed near the bottom boundary for PCA20 and PCAT profiles. The oscillations are the strongest for PCA20 at 28 min, but disappear at later times. This results emphasize the importance of the time control strategy

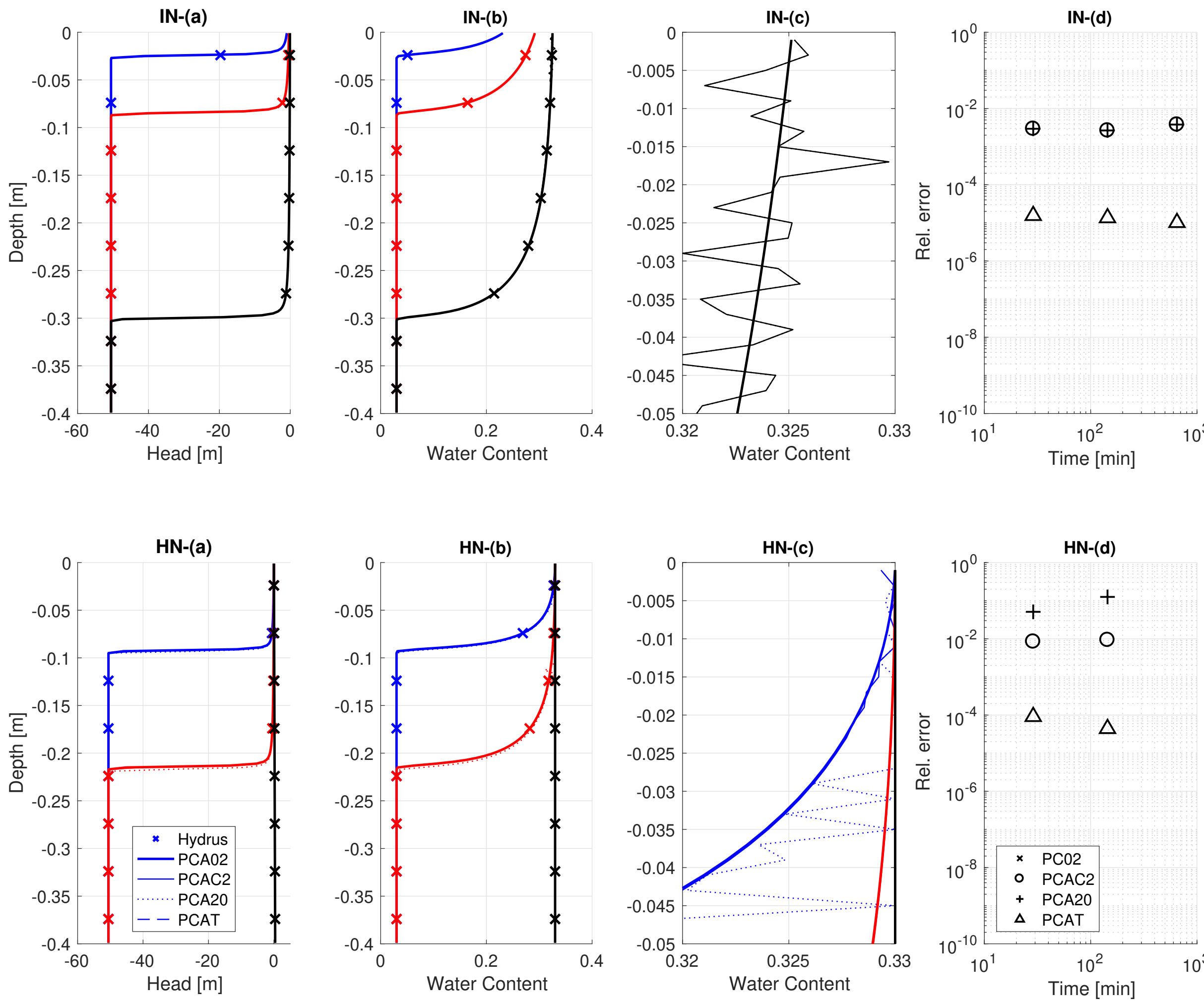

Figure 7: (a): Head and (b): water content profiles for IN and HN scenarios. Blue: $t = 28$ min, Red: $t = 144$ min, Black: $t = 648$ min. The Hydrus results are plotted at coarser resolution for readability. (c): Zoomed water content profiles to show details near the saturated-unsaturated interface. (d): Relative difference in water content (ϵ_θ) for the tested scenarios (taking PCA02 as the reference solution).

particularly when the domain is nearly saturated. It also supports the use of the Courant number criteria that allows larger Δt at low saturation.

The plots of the relative difference show that PCA20 and PCAT have the highest deviations. PCAC2 has relatively low deviations and PC02 has the lowest deviations. As time evolves, relative differences of PCA20 and PCAC2 decrease while PACT shows a different trend. This phenomenon again highlights the distinction between time control strategies under different saturation status and head gradient. For these 2 scenarios, the Courant number criteria successfully reduce model deviation and avoid oscillation.

3.2.4. Computational cost

Figure 9 shows the total number of iterations (i.e. total number of matrix inversion operations performed) for different simulation scenarios. PC02 and PCA02 produce indistinguishable results, so it is not shown. The PCA02 and PCA20 curves are generally consistent among different scenarios because change in Δt is limited by $\Delta t_{\max}$, which is constant among scenarios. Although PCA02 is considered the most accurate solution, it is certainly not an efficient approach. The PCA20 simulations are generally efficient, but it produces oscillatory profiles for IN, HN, NH and EH scenarios. The implication is that time control based on moisture change alone (Eq. 11) does not capture all potential sources for oscillations and instability. Although model performance can be improved by reducing $\Delta t_{\max}$, since no guideline is available for determining the optimal $\Delta t_{\max}$, good computational efficiency and oscillation-free solution are unlikely to be achieved simultaneously without multiple trials.

The PCAT has good computational efficiency for NN, NH, EN and EH scenarios, but its performance on infiltration scenarios are disappointing. The reason is that these scenarios involve large head gradients, which lead to high truncation errors. Without a limitation on $\Delta t_{\max}$, PACT takes much fewer iterations in NN and EN at a cost of higher model error (but remains oscillation-free). For drainage problems (NH and EH), oscillations are observed for PCAT. It can be concluded that (i) time control based on truncation error (Eq. 13)

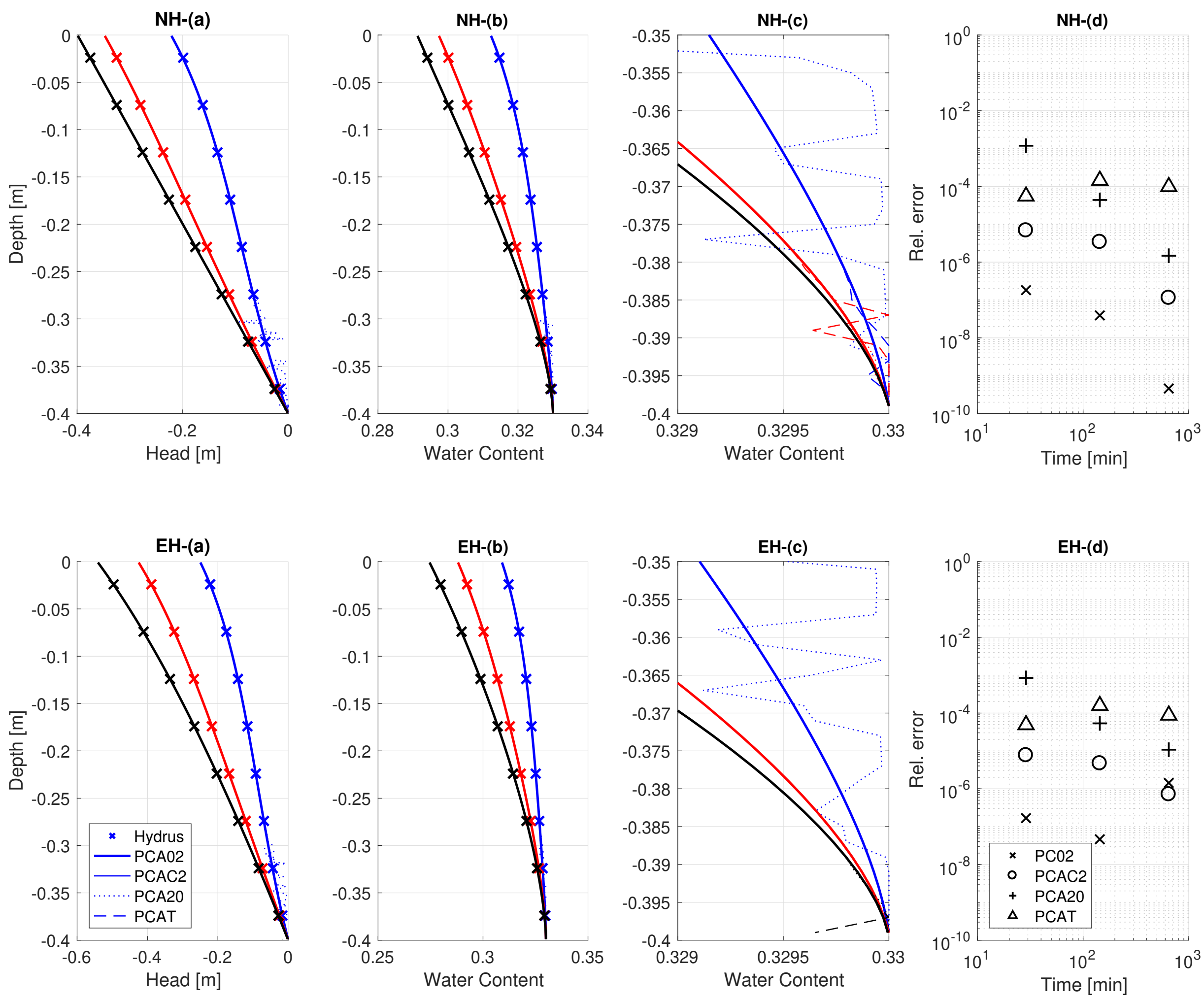

Figure 8: (a): Head and (b): water content profiles for NH and EH scenarios. Blue: $t = 28$ min, Red: $t = 144$ min, Black: $t = 648$ min. The Hydrus results are plotted at coarser resolution for readability. (c): Zoomed water content profiles to show details near the saturated-unsaturated interface. (d): Relative difference in water content (ϵ_θ) for the tested scenarios (taking PCA02 as the reference solution).

is not suitable for problems with drastic head change, and (ii) a $\Delta t_{\max}$ is still needed to restrict oscillations, so it shares the same problem with the moisture criteria (Eq. 11).

For all tested scenarios except IN, the computational cost of PCAC2 lies between PCA02 and PCA20, making it a promising choice that balances accuracy and efficiency. However, it fails to restrict Δt in fully unsaturated domains (e.g. IN), which results same cost as PCA20. The Courant number criteria reduces Δt at high saturation where oscillations are likely to occur, which is the main advantage over the use of constant $\Delta t_{\max}$. But $Co_{\max} = 2$ is not a universally optimal value. More discussion on the Courant number criteria can be found in Sec. 4.

Finally, the heuristic Δt control strategy with Hydrus-1D outperforms the PCAC2 in almost all scenarios. The only exception is the EN scenario (excluding IN that has oscillations), where PCAC2 uses large Δt at late stages because evaporation drives the entire soil column to become unsaturated. We may conclude that a non-iterative scheme is not necessarily more efficient than an iterative scheme. The selection between an iterative and a non-iterative solver could depend on the problem to be solved, the soil properties, the discretization and the desired tolerance level. For example, if relatively large error can be accepted, PCAT is the most efficient method for NN scenario. The Hydrus simulations performed in the present study use the default convergence criteria in the Hydrus-1D software, which is based on the change of both head and water content. We found that if water content is used as the convergence criteria alone, Hydrus takes many more iterations for the infiltration scenarios. There is no universally optimal time control strategy, but the Courant number criteria certainly provides an attractive alternative for the P-C-A method.

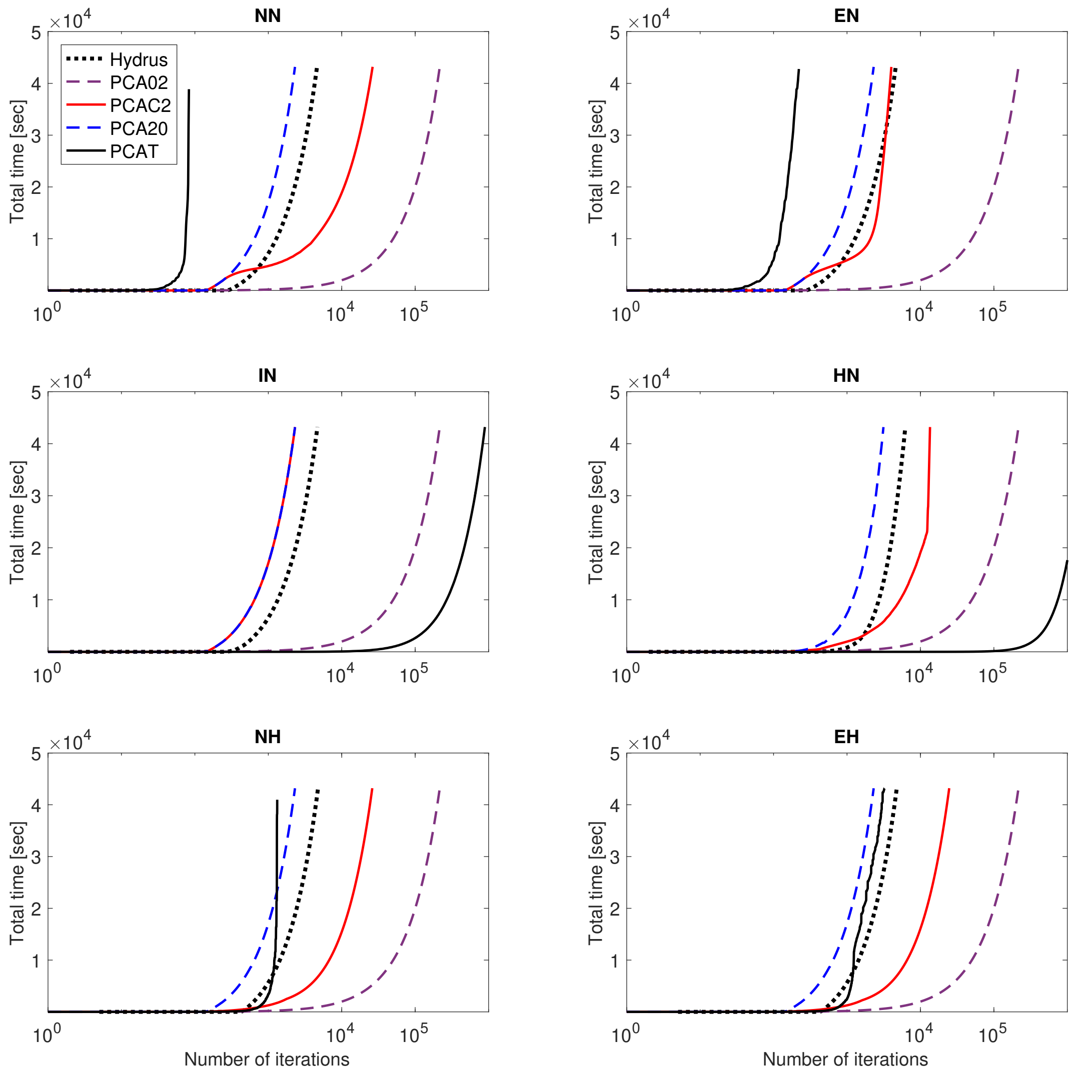

Figure 9: Total number of iterations for all tested scenarios. The x-axis is displayed at log scale.

4. Discussion

4.1. Post-allocation in detail

Post-allocation is a key step of the proposed P-C-A method. To fully understand this process, a toy infiltration problem is investigated (similar to the Warrick's problem, but with fewer grid cells and time steps). The maximum Δt is set to 2 s to intentionally create oscillations. Figure 10 shows the variation of water content in one grid cell (at $z = -0.008$ m) when transitioning from unsaturated to saturated status. This transition does not occur smoothly. Oscillations are observed for both θ^{n+1} and θ^*. For the P-C-A method (Fig. 10a), starting from 100 s, the target cell switches between unsaturated and saturated status multiple times, which corresponds to the oscillations of the water content profile near the saturated-unsaturated interface that we have seen previously (e.g. Fig. 3). During this process, $\theta^{n+1} \leq \theta_s$ always holds and volume loss is avoided. Note that θ^{n+1} shows much weaker oscillation magnitudes that θ^*, indicating the post-allocation scheme helps to stabilize the evolution of water content. It also indicates that the oscillations arise in the explicit corrector step, not the post-allocation step. Thus the key to suppress such oscillations is to reduce Δt when necessary. For the P-C method (Fig. 10b), there exists θ^{n+1} values that exceed θ_s. Truncation of such unrealistic θ values leads to non-conservation.

Figure 10 also displays the volume of water redistributed through different mechanisms during post-allocation. All 3 mechanisms can be found in Fig. 10(a), which are (i) send from over-saturated cells, $\mathrm{Vs}_{\mathrm{sat}}$, (ii) send from unsaturated cells, $\mathrm{Vs}_{\mathrm{uns}}$ and (iii) receive from neighbor cells, Vr (see detailed allocation paths in Fig. 1 and Table 1). The mechanism (ii) is not implemented for the P-C method described in Lai and Ogden (2015), which could be another reason that infiltration is delayed (Fig. 5) and conservation is violated for the P-C method (the first reason is moisture redistribution among fully saturated cells).

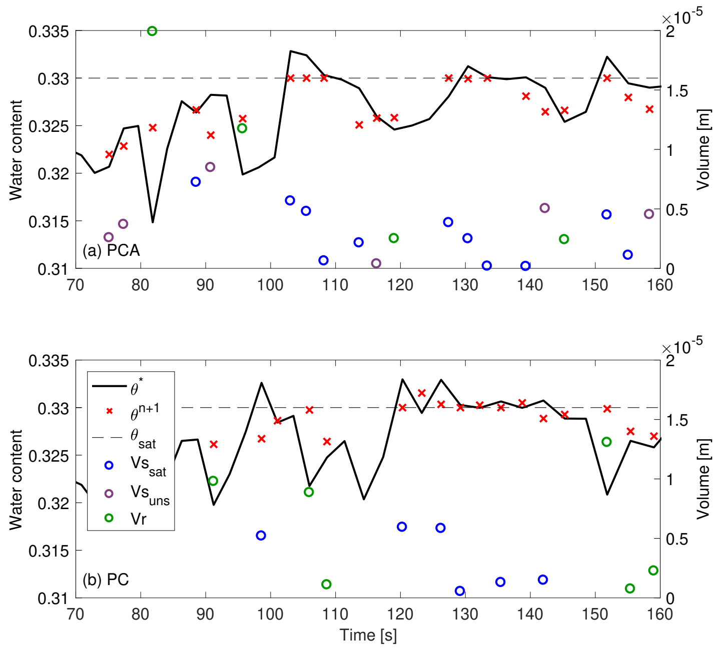

Figure 10: Tracking water content change in one grid cell (at $z = -0.008$ m) before and after post-allocation. (a): P-C-A method. (b): P-C method. $\mathrm{Vs}_{\mathrm{sat}}$, $\mathrm{Vs}_{\mathrm{uns}}$ and Vr are volumes of water that is sent when the target cell is over-saturated, when the target cell is unsaturated and the volume of water that is extracted by the target cell. Note that these volume changes are only triggered by post-allocation of the target cell itself, but the water content update from θ^* to θ^{n+1} is affected by all allocation processes in the entire computational domain, so the allocated volumes (the circle markers) do not necessarily show correlations with $(\theta_{n+1} - \theta^*)$.

4.2. Courant number in detail

The Courant number criteria (Eq. 15) with $Co_{\max} = 2$ generally provides acceptable results, but it could be inadequate for IN and HN, while too conservative for NN and EN scenarios tested in Sec. 3.2. We further find that oscillation-free solutions can be obtained for NN and EN scenarios even with $Co_{\max} = 3$ (not shown), but $Co_{\max} = 0.5$ is required to suppress oscillations for IN and HN (not shown). This result suggests the $Co_{\max}$ is problem-dependent, meaning that not all factors leading to oscillation have been included in the Courant number. Finding the missing factors is reserved for future study. Despite this incompleteness, the Courant number criteria is still useful because (i) for most test scenarios the oscillations are so small that they do not affect the overall shapes of the moisture profile, (ii) variation of the Courant number matches variation of required Δt, where small Δt is automatically obtained at high saturation, and (iii) selecting $Co_{\max}$, which is around 2, is much easier than selecting $\Delta t_{\max}$.

The Courant number criteria is sensitive to the safety factor λ. If we reduce λ to 0.99, oscillations appear in all scenarios even with $Co_{\max} = 0.5$ (not shown). If we increase λ to 1, Δt drops down to $< 1 \times 10^{-4}$ s for the HN scenario (not shown). The effects of λ could depend on the soil characteristics (the shape of $Co - \theta$ curve), future studies that apply the P-C-A method to different types of soils (possibly with heterogeneity) should provide more insight on the role of λ. For the time being, λ is simply used as a constant parameter that balances computational cost and acceptable level of oscillations.

5. Conclusions

The present study focuses on solving one-dimensional Richards equation for variably-saturated groundwater flow. The predictor-corrector (P-C) method proposed by Lai and Ogden (2015) is used with a new post-allocation scheme (named the P-C-A method) to guarantee mass conservation when moisture redistribution occurs in the saturated region. A variety of adaptive time control strategies are tested, including a novel approach that combines the traditional moisture difference criteria with the Courant number criteria. The findings are listed below:

1. The P-C method does not always conserve mass at the saturated-unsaturated interface because it unrealistically allocates excess moisture to fully saturated grid cells. But depending on the problem tested, this non-conservation could be negligible.
2. The new post-allocation scheme is essential for the P-C-A method to guarantee exact mass conservation. It also helps to alleviate oscillations when large Δt is used.
3. Error of the P-C-A method is sensitive to the time step size (Δt). Adaptive time control based on moisture difference (Eq. 11) lacks guidance for the modeler to choose the maximum allowable time step ($\Delta t_{\max}$), which often results either inefficient simulation (with $\Delta t_{\max}$ being too small) or oscillatory solution (with $\Delta t_{\max}$ being too big).
4. Adaptive time control based on truncation error (Eq. 13) can be used when the head gradient is small, otherwise it becomes expensive.
5. Using the Courant number to constrain maximum Δt is promising because it enforces small Δt at high saturation where oscillations are likely to occur. Although the optimal value of $Co_{\max}$ is problem-dependent, determining $Co_{\max}$ is much easier than determining $\Delta t_{\max}$ because $Co_{\max}$ varies within a smaller range. For most problems tested in the present study, a $Co_{\max}$ of 2 is sufficient for the P-C-A method to produce conservative, accurate numerical solution at reasonable computational cost.
6. Non-iterative method does not necessarily have computational advantage over iterative method because a smaller Δt might be required to maintain stability.

References

Camporese, M., Daly, E., Paniconi, C., 2015. Catchment-scale Richards equation-based modeling of evapotranspiration via boundary condition switching and root water uptake schemes. Water Resources Research 51, 5756–5771. doi:10.1002/2015WR017139.

Caviedes-Voullieme, D., Garcia-Navarro, P., Murillo, J., 2013. Verification, conservation, stability and efficiency of a finite volume method for the 1D Richards equation. Journal of Hydrology 480, 69–84. doi:10.1016/j.jhydrol.2012.12.008.

Celia, M., Bouloutas, E., Zarba, R., 1990. A general mass-conservative numerical solution for the unsaturated flow equation. Water Resources Research 26, 1483–1496. doi:10.1029/WR026i007p01483.

van Dam, J., Feddes, R., 2000. Numerical simulation of infiltration, evaporation and shallow groundwater levels with the richards equation. Journal of Hydrology 233, 72–85. doi:10.1016/S0022-1694(00)00227-4.

D'Haese, C., Putti, M., Paniconi, C., Verhoest, N., 2007. Assessment of adaptive and heuristic time stepping for variably saturated flow. International Journal for Numerical Methods in Fluids 53, 1173–1193. doi:10.1002/fld.1369.

El-Kadi, A., Ling, G., 1993. The courant and peclet number criteria for the numerical solution of the richards equation. Water Resources Research 29, 3485–3494. doi:10.1029/93WR00929.

Farthing, M., Ogden, F., 2017. Numerical solution of Richards' equation: A review of advances and challenges. Soil Science Society of America Journal 81, 1257–1269. doi:10.2136/sssaj2017.02.0058.

Forsyth, P., Wu, Y., Pruess, K., 1995. Robust numerical methods for saturated-unsaturated flow with dry initial conditions in heterogeneous media. Advances in Water Resources 18, 25–38. doi:10.1016/0309-1708(95)00020-J.

van Genuchten, M., 1980. A closed-form equation for predicting the hydraulic conductivity of unsaturated soils. Soil Science Society of America Journal 44, 892–898. doi:10.2136/sssaj1980.03615995004400050002x.

Hirsch, C., 2007. Numerical Computation of Internal and External Flows: The Fundamentals of Computational Fluid Dynamics. 2 ed., Butterworth-Heinemann, Burlington, MA, USA.

Hunter, N.M., Horritt, M.S., Bates, P.D., Wilson, M.D., Werner, M.G.F., 2005. An adaptive time step solution for raster-based storage cell modelling of floodplain inundation. Advances in Water Resources 28, 975–991.

Kavetski, D., Binning, P., Sloan, S., 2002. Noniterative time stepping schemes with adaptive truncation error control for the solution of richards equation. Water Resources Research 38, 1211. doi:10.1029/2001WR000720.

Kirkland, M., Hills, R., Wierenga, P., 1992. Algorithms for solving Richards' equation for variably saturated soils. Water Resources Research 28, 2049–2058. doi:10.1029/92WR00802.

Lai, W., Ogden, F., 2015. A mass-conservative finite volume predictor-corrector solution of the 1D Richards' equation. Journal of Hydrology 523, 119–127. doi:10.1016/j.jhydrol.2015.01.053.

Lehmann, F., Ackerer, P., 1998. Comparison of iterative methods for improved solutions of the fluid flow equation in partially saturated porous media. Transport in Porous Media 31, 275–292. doi:10.1023/A:1006555107450.

Li, Z., Hodges, B., 2019. Model instability and channel connectivity for 2D coastal marsh simulations. Environmental Fluid Mechanics 19, 1309–1338. doi:10.1007/s10652-018-9623-7.

Maina, F., Ackerer, P., 2017. Ross scheme, Newton-Raphson iterative methods and time-stepping strategies for solving the mixed form of Richards' equation. Hydrology and Earth System Sciences 21, 2667–2683. doi:10.5194/hess-21-2667-2017.

Maquin, M., Mouche, E., Mugler, C., Pierret, M., Viville, D., 2017. A soil column model for predicting the interaction between water table and evapotranspiration. Water Resources Research 53, 5877–5898. doi:10.1002/2016WR020183.

Mualem, Y., 1976. A new model for predicting the hydraulic conductivity of unsaturated porous media. Water Resources Research 12, 513–522. doi:10.1029/WR012i003p00513.

Or, D., Lehmann, P., Shahraeeni, E., Shokri, N., 2013. Advances in soil evaporation physics - A review. Vadose Zone Journal 12. doi:10.2136/vzj2012.0163.

Paniconi, C., Putti, M., 2015. Physically based modeling in catchment hydrology at 50: Survey and outlook. Water Resources Research 51, 7090–7129. doi:10.1002/2015WR017780.

Phoon, K., Tan, T., Chong, P., 2007. Numerical simulation of Richards equation in partially saturated porous media: under-relaxation and mass balance. Geotechnical and Geological Engineering 25, 525–541. doi:10.1007/s10706-007-9126-7.

Richards, L.A., 1931. Capillary conduction of liquids through porous mediums. Physics 1, 318–333.

Simunek, J., Sejna, M., Saito, H., Sakai, M., van Genuchten, M., 2009. The HYDRUS-1D software package for simulating the one-dimensional movement of water, heat and multiple solutes in variably-saturated media. Department of Environmental Sciences, University of California Riverside, Riverside, CA .

Sun, X., Bernard-Jannin, L., Garneau, C., Volk, M., Arnold, J., Srinivasan, R., Sauvage, S., Sanchez-Perez, J., 2016. Improved simulation of river water and groundwater exchange in an alluvial plain using the SWAT model. Hydrological Processes 30, 187–202. doi:10.1002/hyp.10575.

Warrick, A., Lomen, D., Yates, S., 1985. A generalized solution to infiltration. Soil Science Society of America Journal 49, 34–38. doi:10.2136/sssaj1985.03615995004900010006x.

Weill, S., Altissimo, M., Cassiani, G., Deiana, R., Marani, M., Putti, M., 2013. Saturated area dynamics and streamflow generation from coupled surface-subsurface simulations and field observations. Advances in Water Resources 59, 169–208. doi:10.1016/j.advwatres.2013.06.007.

Zha, Y., Yang, J., Yin, L., Zhang, Y., Zeng, W., Shi, L., 2017. A modified Picard iteration scheme for overcoming numerical difficulties of simulating infiltration into dry soil. Journal of Hydrology 551, 56–69. doi:10.1016/j.jhydrol.2017.05.053.

Zha, Y., Yang, J., Zeng, J., Tso, C., Zeng, W., Shi, L., 2019. Review of numerical solution of Richardson-Richards equation for variably saturated flow in soils. WIREs Water 6(5). doi:10.1002/wat2.1364.